PAPER

Check for updates

An improved method to generate secondary nanoplastics and oligomers: application in ecotoxicology†

Silvia Gómez-Kong, [iD] ‡[a] Miguel Tamayo-Belda,‡[a] Gerardo Pulido-Reyes, [iD] [a] Carlos Edo,[b] Irene Verdú,[a] Francisco Leganés,[ac] Roberto Rosal, [iD] [b] Miguel González-Pleiter [iD] [ac] and Francisca Fernández-Piñas [iD] ★[ac]

Recent studies have highlighted the ecotoxicological effects of conventional primary nanoplastics (NPLs); however, the impacts of secondary NPLs and oligomers (Olig), especially those derived from biodegradable plastics, formed through fragmentation and natural degradation processes (*e.g.*, photooxidation) remain underexplored. This gap is partly due to challenges in producing sufficient quantities for toxicity testing. An improved method to generate non-photooxidized (NP) and photooxidized (P) secondary NPLs and Olig from polybutylene adipate *co*-terephthalate (PBAT), a biodegradable plastic commonly used in agriculture mulching, which involves the mechanical breakdown of PBAT-microbeads with or without prior photooxidation is presented. PBAT was irradiated at ~9.34 kW m^{-2} (approximately 120 times the solar irradiance) for 96 h, irradiation that corresponds to ~16 months of average sunlight in the Iberian Peninsula (7.7 kWh m^{-2} per day). The toxicological effects on *Chlamydomonas reinhardtii*, a model green microalga of primary producers in freshwater ecosystems, were also assessed. The protocol yielded 0.199 mg of secondary NP-PBAT-NPLs and 10.275 mg of NP-PBAT-Olig per gram of PBAT-microbeads. PBAT-NPLs presented irregular spherical morphologies and hydrodynamic sizes ranging from 56.71 to 69.86 nm. HPLC and MALDI-TOF analysis identified linear and cyclic Olig, ranging from dimers to 19 repeated-units Olig. PBAT-NPLs and PBAT-Olig exhibited negative surface charges, suggesting colloidal stability in water. While PBAT-NPLs and PBAT-Olig did not inhibit algal growth in the short term, they induced reactive oxygen species overproduction at the environmentally relevant concentration of 0.01 mg L^{-1} and caused membrane depolarization, impaired photosynthesis and lipid peroxidation at 10 mg L^{-1}. Non-photooxidized PBAT-NPLs exhibited the highest toxicity, followed by photooxidized PBAT-NPLs and both non-photooxidized and photooxidized PBAT-Olig. This study provides an efficient method for producing reference secondary NPLs and Olig and underscores the potential risks of PBAT towards primary producers in freshwater ecosystems.

Environmental significance

This work presents an improved method to produce secondary nanoplastics (NPLs) and oligomers (Olig), both photooxidized and non-photooxidized, which may be applicable to generate reference NPLs in sufficient quantities and realistic morphologies to study their impact on the biota. In addition, the production and characterization of generated Olig might be useful to further characterize the complete fragmentation of larger plastic fractions in the environment and assess their environmental impact which is a topic largely unexplored. The generated materials were tested in the microalga *Chlamydomonas reinhardtii*, a primary producer relevant in freshwater. Alterations in the main physiological parameters of the alga were found at environmentally relevant NPL concentrations meaning that, in the long term, the aquatic trophic chain might be compromised.

[a] *Department of Biology, Faculty of Science, Universidad Autónoma de Madrid, E-28049, Madrid, Spain. E-mail: francisca.pina@uam.es*
[b] *Department of Chemical Engineering, Universidad de Alcalá, E-28871 Alcalá de Henares, Madrid, Spain*
[c] *Centro de Investigación en Biodiversidad y Cambio Global (CIBC-UAM), Universidad Autónoma de Madrid, C Darwin 2, 28049 Madrid, Spain*
† Electronic supplementary information (ESI) available. See DOI: https://doi.org/10.1039/d4en00866a
‡ These authors contributed equally to this work.

1 Introduction

In total, 1925 million tons of plastics were produced worldwide between 2018 and 2022, excluding quantities used for adhesives, sealants, coatings, paints, varnishes, textiles, and waterproofing, or those for the production of cosmetics and medicines.[1] Notably, approximately 90% of these plastics were derived from fossil fuels, while less than 9% originated

1150 | *Environ. Sci.: Nano*, 2025, **12**, 1150–1165

This journal is © The Royal Society of Chemistry 2025

from recycling processes.[1] During this same period, the production of bio-based plastics doubled, reaching 2.3 million tons in 2022.[1] The majority of plastics are utilized in packaging,[1] which typically results in a short product lifespan. Once discarded, plastic waste can follow several pathways: recycling (only for some types and a limited number of times), landfill disposal, energy recovery or release into the environment upon entering either directly or after undergoing one or more of these processes. Calculations suggest that between 0.8 and 2.7 Mt enter the ocean each year and 80% of them are transported by rivers threatening freshwater ecosystems.[2]

Freshwater ecosystems serve as key pathways for the transport of plastic waste into the environment.[3] Upon entering the ecosystems, it undergoes fragmentation and natural degradation processes due to factors such as light (producing photooxidation), temperature (producing thermal oxidation), water (producing hydrolysis) or mechanical forces, with the latter generally considered the most efficient abiotic degradation procedure.[4] Exposure to visible and ultraviolet radiation increases the plastic reactivity by promoting electron excitation, which accelerates oxidation, cleavage, and chain scission, leading to the formation of smaller particles in the nanometer range.[5] These particles, known as nanoplastics (NPLs; plastic particles < 1000 nm in one dimension[6]), frequently appear together with oligomers (Olig: short polymeric chains) that are released during the same degradation process and may be isolated by ultrafiltration through 50 kDa MWCO (molecular weight cut-off).[7,8] On the one hand, particles smaller than 1000 nm tend to remain as stable colloidal systems unless the particles exhibit neutral surface charge (absolute ζ-potential values of 20–30 mV or higher are generally accepted to maintain colloidal stability).[9] On the other hand, the behaviour of molecules is influenced by several factors, mainly their interaction with the surrounding solvent that may promote their solubility or more frequently, in aqueous media, their hydrophobic-driven self-aggregation.[10] Furthermore, NPLs and Olig can be categorized by origin into primary which are intentionally manufactured, such as those found in personal care products, and secondary resulting from fragmentation and degradation of macro and microplastics into nanosized particles.[11]

Research on the presence of NPLs in the environment remains limited due to the technical challenges associated with their identification and quantification in complex matrices.[12,13] To date, the presence of NPLs in the environment has been analyzed using different techniques such as adapted thermal desorption proton transfer reaction mass spectrometry (TD-PTR-MS[14–19]) and pyrolysis gas chromatography mass spectrometry (PY-GC/MS[20–22]). The concentration of NPLs in different water bodies ranges from 0.1 μg L^{-1} (ref. 20–22) in river waters, groundwater and WWTP water effluents in China to an extreme value of 1588 μg L (ref. 17) in a Swedish lake. Despite these findings and the potential higher degradation rates of biodegradable NPLs, there is currently no evidence of biodegradable NPLs or oligomers in the environment.[23]

Due to these barriers for NPL identification and aiming at evaluating the physicochemical behavior and biological toxicity of NPLs in complex matrices, some studies have focused on generating different types of NPLs to tackle these handicaps. Most of them have applied a variety of bottom-up methods to obtain NPLs for different applications: testing different materials such as PMMA (polymethyl methacrylate) or PHB (polyhydroxybutyrate)[24,25] and making NPLs trackable[26,27] and with more realistic irregular shapes.[28,29] There exist alternatives for top-down methods producing more realistic NPLs by mechanical fragmentation of larger plastics in different liquid media,[30–32] as well as through laser ablation.[33] These alternatives have not only allowed the use of different materials in the NPL toxicology but also brought to light the lack of standardized methodologies to produce high quantities of realistic NPLs of reference that behave in a similar way to those naturally occurring in the environment as a consequence of the degradation processes of larger plastics.[4]

Once NPLs reach the environment, they can exert negative effects on organisms. To the best of our knowledge, so far effects of secondary NPLs, at environmentally relevant concentrations, on the viability of organisms have not been described, but they have been described for more sensitive endpoints such as specific metabolic alterations and behavioral changes.[32,34] In this regard, environmental risk could be underestimated. In general, toxicological studies about NPLs have predominantly focused on evaluating a few types of primary NPLs such as PS (polystyrene), PE (polyethylene) and PMMA.[35–41] In comparison, conventional polymers and biopolymers appear to exert similar toxicity.[42] However, the faster degradation of the biopolymers, with the greater release of additives, and their effects on the biota and their balance may jeopardize to a greater extent the stability of the ecosystems.[43,44] Only a limited number of scientific articles have examined the impact of secondary NPLs or/and biodegradable plastics like PCL (polycaprolactone),[8] PHB[7,25] and PLA (polylactic acid).[32] The uncontrolled release of plastic oligomers has been considerably studied as non-intentionally added substances in food contact materials,[45] but their impact on the environment is an issue that has yet to be addressed.

Taken together, while there is a rapidly growing body of evidence on the presence of NPLs in the environment and the negative effects of primary NPLs, standard methods to detect NPLs in complex matrices are still under development and studies assessing the effects of secondary NPLs and Olig (especially those derived from biodegradable plastics) formed through fragmentation and natural degradation processes (e.g., photooxidation) remain scarce. These knowledge gaps are partly due to the challenges of producing sufficient quantities for toxicity and analytical testing. Here, we have developed a highly efficient method to generate both non-photooxidized and photooxidized secondary NPLs and Olig from polybutylene adipate co-terephthalate (PBAT) – a biodegradable plastic commonly used in agriculture mulching – which can be adapted to other polymers. Our novel method involves the mechanical breakdown of pristine PBAT-microbeads, with or

This journal is © The Royal Society of Chemistry 2025

Environ. Sci.: Nano, 2025, 12, 1150–1165 | 1151

without prior photooxidation. The toxicological effects on *Chlamydomonas reinhardtii* (*C. reinhardtii*), a model green microalga of primary producers in freshwater ecosystems, were also assessed.

2 Materials and methods

2.1 Nanoplastic and oligomer production

Secondary non-photooxidized (NP-) PBAT nanoplastics (PBAT-NPLs) and PBAT oligomers (PBAT-Olig) have been produced

by mechanical breakdown of commercial PBAT microbeads purchased from Ecoflex with an average molecular number of ~50 kDa.[46] 300 g of commercial microbeads were frozen with liquid nitrogen at −140 °C and triturated in a modified stainless-steel blender Thermomix TM31 (Vonwerk, Germany) equipped with four stainless-steel blades and a load capacity of 1.3 L (ESI† Text S1 Fig. 1). The trituration was carried out for 1 minute at a speed of 10 000 rpm and passed through a 1 mm sieve, to isolate the smaller fractions. 10 trituration cycles were done only in the plastic fraction >1 mm. At the
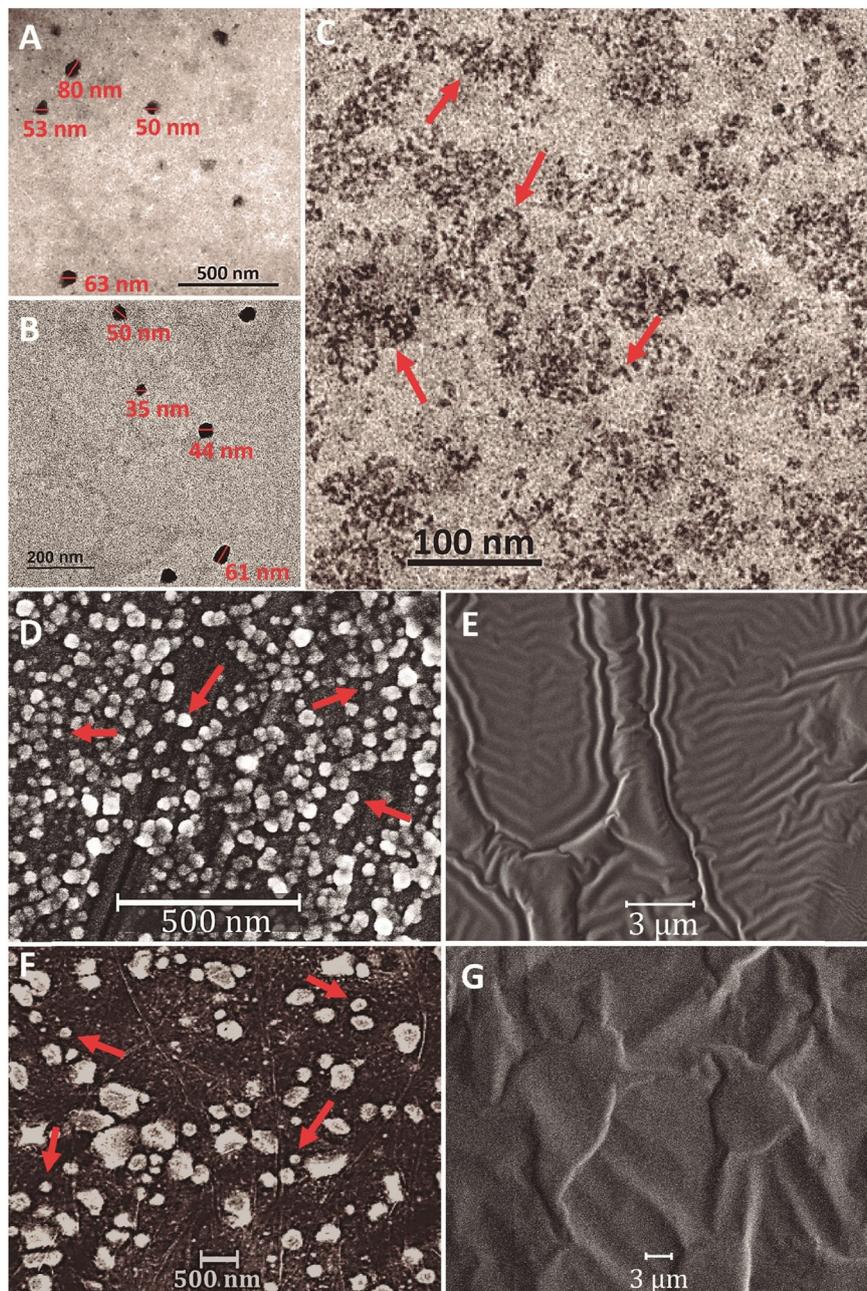
Fig. 1 A) Transmission electron microscopy (TEM) image of NP-PBAT-NPLs. B) TEM image of P-PBAT-NPLs. C) TEM image of NP-PBAT-Olig. D) Scanning electron microscopy (SEM) image of NP-PBAT-NPLs. E) SEM image of NP-PBAT-Oligomers. F) SEM image of P-PBAT-NPLs. G) SEM image of P-PBAT-Oligomers. Red arrows indicate individual particles.

end of the trituration procedure, approximately 70% of the plastic was smaller than 1 mm.

15 g of the pulverized plastic <1 mm was collected, resuspended in 20 mL of absolute ethanol and 60 mL of ultra-pure water and then ultrasonicated on a Branson Ultrasonics™ Sonifier™ S-450A (Branson Ultrasonics Co., Brookfield, CT, USA) for 2 min at 60% duty cycle and 260 W. Then, the resuspended fraction was filtered using a 1 μm pore nylon filter (filters were replaced every 100 mL). Fractions below 1 micron were concentrated, and the oligomeric fraction was separated by centrifuge ultrafiltration using a 50 kDa MWCO membrane. Both fractions between 5 and 1000 nm and fractions <5 nm (50 kDa MWCO), hereinafter named NP-PBAT-NPLs and NP-PBAT-Olig, respectively, were dried in a previously cleaned oven used only for this purpose at 60 °C for 48 hours, and then weighed using a balance (accuracy ± 0.01 mg), and stored in 4 mL glass flasks for later use.

Secondary photooxidized (P-) PBAT nanoplastics (PBAT-NPLs) and PBAT oligomers (PBAT-Olig) were produced as follows: 100 g of commercial PBAT microbeads were place into a glass bottle filled with 800 mL of absolute ethanol and then radiated with a 150 W medium-pressure mercury lamp (Novalight TQ150) emitting in the 297–579 nm range for 96 h (Text S1† Fig. 2), irradiation that corresponds to ~16 months of average sunlight in the Iberian Peninsula (7.7 kWh m^{-2} per day).[47] After radiation, microbeads were filtered and dried, and the same protocol for the production of NP-PBAT-NPLs and NP-PBAT-Olig was conducted. Detailed information about the protocols described above is available in the ESI† (Text S1).

2.2 Physicochemical characterization

2.2.1 Dynamic light scattering (DLS) and electrophoretic light scattering (ELS).
The hydrodynamic size and surface charge (inferred using the ζ-potential) of the colloidal suspension of NP- and P-PBAT-NPLs and NP- and P-PBAT-Olig were determined by DLS and ELS using a Zetasizer® Nano ZS (Malvern Instruments, Malvern, UK). Measurements were performed at 25 °C in ultra-pure water and in the corresponding culture medium used for the biological study. A working suspension of 1000 mg L^{-1} of each material was used. Additionally, to investigate the influence of the culture medium in the NPL dispersion, the same concentrations were prepared in the appropriate culture medium. DLS measurements were replicated five times with eleven runs per replicate, while ELS measurements were replicated five times with thirty runs per replicate.

2.2.2 Transmission and scanning electron microscopy (TEM/SEM).
For transmission electron micrographs, 10 μl of 1000 mg L^{-1} PBAT-NPL suspension was placed on a carbon film coated, 400 mesh, nickel grid support and dehydrated at room temperature to fix the material on the grid. Post-fixation was performed in osmium tetroxide in phosphate buffer for 2 h at 4 °C. Samples were stained with 2% uranyl acetate. PBAT-NPLs were visualized on a JEOL (JEM 1010) electron microscope (80–120 kV). For scanning electron images (SEM), working suspensions of 100 mg L^{-1} NP- and P-PBAT-NPLs or PBAT-Olig were prepared from which 10 μL was placed on an aluminum holder, dehydrated at room temperature and coated with 5 nm of chromium. Samples were studied using electron beam lithography eLINE-Plus equipment (Raith, Germany).

2.2.3 Fourier transform infrared spectroscopy (FTIR).
The identification of the chemical structure of PBAT-NPLs and PBAT-Olig obtained at different stages of the production process was performed by attenuated total reflectance Fourier transform infrared (ATR-FTIR) spectroscopy. Commercial PBAT microbeads, fragmented materials below 1 mm obtained after mechanical breakdown, nanoparticle samples and oligomer samples were analysed and compared. PBAT-NPL and PBAT-Olig samples were dried at 60 °C and placed over the ATR-crystal. For the microbeads, a slice was cut and placed over the ATR-crystal. Spectra were taken in the 4000–500 cm^{-1} range. The analysis was conducted on a Perkin-
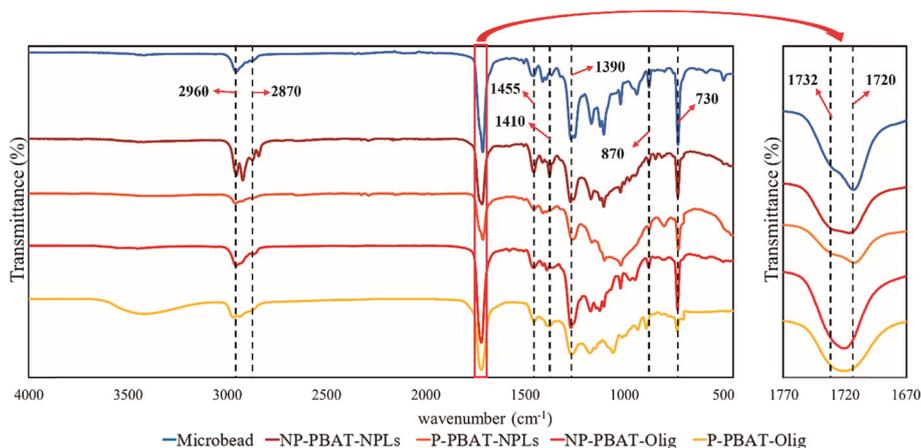

Fig. 2 Infrared spectra of NP- and P-PBAT-NPLs and NP- and P-PBAT-Olig and the initial material (PBAT microbeads).

Elmer Spotlight 200 Spectrum Two apparatus equipped with an MCT detector (PerkinElmer, USA). The IR spectra were analysed using Origin software (OriginLab Corporation, USA).

2.2.4 High-performance liquid chromatography (HPLC) and matrix-assisted laser desorption/ionization (MALDI) time-of-flight/time-of-flight (TOF/TOF) mass spectrometry. Considering the wide variety of oligomers that may potentially appear in the NP- and P-PBAT-Olig samples, the characterization of this fraction was conducted in two steps: separation by polarity of the different oligomeric compounds present in the raw NP- and P-PBAT-Olig materials generated (which mainly depends on the hydrocarbon chain length and monomer composition) followed by individual MALDI-TOF/TOF analysis of each peak obtained in the first step. Chromatographic separation of the raw NP- and P-PBAT-Olig materials was conducted using an HPLC 1200 Series Agilent apparatus (Agilent Technologies, Germany) equipped with an autosampler and ultraviolet diode array detector. The raw material was separated on an Ace Excel 5 CN-ES (250 × 4.6 mm, 5 μm) column with 100% methanol as a mobile phase at a flow rate of 1 mL min^{-1} with a 0–20 min gradient.

The material was injected at 20 mg mL^{-1} and analysed at 254 nm. The oligomeric chain length and structure were assessed by mass spectrometry with a MALDI-TOF/TOF configuration and a NdYAG laser (355 nm) ULTRAFLEX III (Bruker Daltoniks GmbH, Bremen, Germany). MALDI TOF/TOF analyses were performed essentially as described by Tamayo-Belda et al.[8] Each chromatography peak previously separated by polarity in HPLC was dissolved in methanol from which 5 μL of each of the solutions was mixed with 20 μL of trans-2-[3-(4-tert-butylphenyl)-2-methyl-2-propenylidene]malononitrile (DCTB) matrix solution (8 mg mL^{-1} in dichloromethane) and 0.5 μL of sodium iodide (2 mg mL^{-1} in acetone). Before analysis, 0.5 μL of this mixture was placed on the MALDI sample plate to dry at room temperature. Recordings were conducted in positive ion detection mode in the range of 50 to 5000 Da for the most polar peaks and 600 to 5000 Da for the less polar peaks to gain sensitivity. Analyses were performed using FlexAnalysis software (Bruker) complemented with the optimization tool Excel Solver (Microsoft).

2.3 Toxicity bioassay

The unicellular green microalga C. reinhardtii was obtained from the Culture Collection of Algae and Protozoa of Dunstaffnage Marine Laboratory (Scotland, UK) and routinely cultured in six-fold diluted TAP culture medium adjusted at pH 7 and buffered with 3.3 mM tris(hydroxymethyl)aminomethane (TRIS) and 45 mM phosphate buffer. TAP/6 has been used as the appropriate culture medium for growing C. reinhardtii exposed to nanoparticles as described elsewhere[48] in a rotary shaker, at 135 rpm and 28 °C under continuous light of 40 μmol photons m^{-2} s^{-1}. The initial OD$_{750nm}$ for the exposure experiment was 0.15. Microalgae were exposed for 72 h to (1) NP- and P-PBAT-NPLs and (2) NP- and P-PBAT-Olig at different nominal concentrations, hereinafter, concentrations (0.01; 0.1;

1; 10; and 50 mg L^{-1}). Microalgae exposed to the same concentrations of pure ethanol used to resuspend both NPLs and Olig were used as controls (0.01% v/v). Five replicates of controls and three replicates of each treatment were carried out. After 72 h of exposure, cellular growth and the total content of chlorophyll (Chl a + Chl b) were measured. For cellular growth, absorbance at 750 nm was measured. For chlorophyll contents, the photosynthetic pigments were extracted in acetone (90%) at 4 °C for 24 h in the dark, and the absorbance at 664 and 647 nm for Chl a and Chl b, respectively, was measured. The concentration of chlorophylls was determined according to Jeffrey and Humphrey.[49] The pH of the culture medium with and NP- and P-PBAT-Olig was measured after 96 h to ensure that no toxic effects were observed due to the medium acidification (Table S1†).

2.3.1 Flow cytometry analyses. The mechanisms of action of NP- and P-PBAT-NPLs and NP- and P-PBAT-Olig on the alga were measured in C. reinhardtii cultures, exposed for 72 h at concentrations of 0.01, 0.1, 1, 10, and 50 mg L^{-1} of each fraction, in triplicate using flow cytometry (FCM) in a CytoFLEX S flow cytometer (Beckman Coulter) fitted with violet (405 nm), blue (488 nm), yellow-green (561 nm), and red (638 nm) lasers. The size was detected with forward scattering (FSC), and a blue laser with three detectors with different wavelength intervals was used: a 488/8 nm detector of side scattering (SSC), 525/40 nm (FITC), and 690/50 nm (PerCP). Besides the size (FSC), complexity (SSC) and chlorophyll autofluorescence (PerCP), two fluorescent probes (FITC) were used to evaluate two physiological parameters (incubation times and concentrations were adapted from Tamayo-Belda et al.):[50] dihydrorhodamine 123 (DHR 123) for the measurement of intracellular reactive oxygen species (ROS) and bis-(1,3-dibutylbarbituric acid) trimethine oxonol (DiBAC4(3)) for the detection of changes in cytoplasmic membrane potential. Specific information, concentration, incubation times and channels are described in Table S2.† All fluorochrome stock solutions were prepared in dimethyl sulfoxide and stored at −20 °C. Fluorescence was analysed in logarithmic mode and at least 20 000 gated cells with similar sizes and complexities were evaluated. Three independent experiments with six controls and three samples by treatment were carried out for each parameter. Data acquisition and processing were performed using CytExpert software (Beckman).

2.3.2 Lipid peroxidation. Lipid peroxidation was determined by quantifying thiobarbituric acid reactive substances (TBARS) following the protocol described by Ortega-Villasante et al.[51] with minor modifications. C. reinhardtii cells were centrifuged (10 000 rpm) and resuspended in 1 mL of 0.5% thiobarbituric acid (TBA) in 20% trichloroacetic acid (TCA). The mixture was heated at 90 °C in a hot block for 30 min. Next, samples were centrifuged at 12 000 rpm for 10 min. The absorbance of the supernatant was measured at 532 nm. The value for nonspecific absorbance at 600 nm was subtracted. The amount of TBARS was calculated based on the extinction coefficient of 155 mM^{-1} cm^{-1}. Five replicates of controls and three replicates of each treatment were carried out. Results were expressed as the

percentage of malondialdehyde (MDA) content with respect to the control.

2.3.3 Photosynthesis. The measurement of the photosynthetic oxygen evolution was performed at 28 °C exposing the cells to saturating actin light (300 μmol photons m^{-2} s^{-1}) in a Clark-type oxygen electrode (Hansatech) according to Leganés et al.[52] Five replicates of controls and three replicates of each treatment were carried out. Photosynthetic rates were relativized to the total chlorophyll content and represented as percentage with respect to the control.

2.4 Data analysis

For the biological assays, means and standard error values were calculated for each treatment from three independent replicate experiments. All values were corrected for control values to minimise the effects of external factors. To determine significant differences among test treatments, data were statistically analysed by conducting an overall one-way analysis of variance (ANOVA) using SigmaPlot v11.0 software (Systat Software Inc., USA). $p < 0.05$ was considered statistically significant. When significant differences were observed, Dunnett's multiple comparison post hoc tests were run for comparing treated groups with the controls.

3 Results

3.1 PBAT-NPL and PBAT-Olig characterization

The physicochemical characterization of PBAT-NPLs in terms of size, morphology, surface charge, chemical nature and mass was performed by dynamic light scattering (DLS), scanning electron microscopy (SEM-EDX), electrophoretic light scattering (ELS), Fourier transform infrared spectroscopy (FTIR) and dry weight analysis.

Hydrodynamic size and ζ-potential measurements were carried out in ultra-pure water and culture medium in the absence of cells (Table 1). The concentration used for measurements was 100 mg L^{-1} for all different treatments. DLS measurements in ultra-pure water of both NP- and P-PBAT-NPL hydrodynamic sizes, transformed into number distribution, have mean sizes of 64 ± 5 nm. In the case of NP-PBAT-Olig particles, the mean size was 94 ± 7 nm and 170 ± 8 nm for P-PBAT-Olig, indicating the aggregation of NP- and P-PBAT-Olig in a micellar way due to the high hydrophobicity of the material. Regarding ELS measurements, the ζ-potential of NP- and P-

PBAT-NPLs was −34 mV and −35 mV, respectively, in ultra-pure water at pH 7, indicating a stable colloidal suspension, and −21 mV and −26 mV for NP- and P-PBAT-Olig, respectively, indicating the stability of the micellar aggregates of PBAT-Olig.

The NP-PBAT-NPL sizes found by DLS in ultra-pure water (Table 1; Fig. S1†) were also observed by TEM (Fig. 1A and B), while in P-PBAT-NPLs, some particles seem to be larger probably due to their aggregation during the sample preparation process. Both NP- and P-PBAT-NPL SEM images revealed irregular sphere morphologies, while NP- and P-PBAT-Olig SEM images showed a layer of an oily phase without any visible particle.

The comparative infrared spectra of PBAT microbeads, NP- and P-PBAT-NPLs and NP- and P-PBAT-Olig (Fig. 2) showed characteristic peaks of PBAT. The peaks at 2960 and 2873 cm^{-1} are due to asymmetric and symmetric stretching vibrations for CH_2 groups, respectively. The main shoulder of the carbonyl region (1720 cm^{-1}) is due to strong C=O stretching, while the 1732 cm^{-1} peak corresponds to C=O stretching in carbonyl groups in the amorphous region of the polymer; the latter is absent in NP- and P-PBAT-Olig. The peak at 1455 cm^{-1} is characteristic of C–C stretching in the phenylene group. The peaks at 1410 and 1390 cm^{-1} are due to trans –CH_2– plane bending vibrations and the strong peaks at 1268 cm^{-1} correspond to C–O asymmetric stretching. Finally, the peaks at 870 and 730 cm^{-1} are due to the out of plane phenyl ring bending.[53]

The formulas, structures and lengths of the polymeric series found by MALDI-TOF/TOF in the NP- and P-PBAT-Olig samples are compiled in Table 2. The polymeric series composition varies depending on the structure (linear or cyclic), on the number of butylene-terephthalate units inserted into the oligomers, on the abundance of butylene by-products (butane or butanediol), and on the occurrence of additional carbonyl/hydroxyl groups due to oxidation processes. Both types of PBAT-Olig, non-protoxidized and protoxidized, contained oligomeric materials below 4000 Da. The mean molecular weight of the NP-PBAT-Olig (1971 ± 116 Da) was significantly higher than that of the P-PBAT-Olig (1635 ± 133 Da) as well as the maximum monomer number observed, which reached 19 units in the non-photooxidized and 15 in the photooxidized one. Based on the MALDI-TOF/TOF intensity output (Fig. S2 and S3†), the butylene adipate cyclic dimer exhibited an intensity one order of magnitude higher in P-PBAT-Olig (Fig. S3A†) compared to

Table 1 Hydrodynamic size (Size$_H$), polydispersity index (PdI) and ζ-potential of NP- and P-PBAT-NPLs and NP- and P-PBAT-Olig both in ultrapure water and algal culture medium (TAP/6). Data obtained from 3 independent replicates ± standard deviation. Size distribution curves are available in the ESI† (Fig. S1)

	Size$_H$ in ultra-pure water by number (nm)	PdI in ultra-pure water	ζ-Potential in ultra-pure water (mV)	Size$_H$ in culture media by number (nm)	PdI in culture media	ζ-Potential in culture media (mV)
NP-PBAT-NPLs	64.24 ± 5	0.28	−34.20 ± 2	94.28 ± 7	0.33	−41.00 ± 3
P-PBAT-NPLs	63.50 ± 5	0.21	−35.20 ± 2	59.92 ± 3	0.21	−36.10 ± 2
NP-PBAT-Olig	94.41 ± 7	0.33	−21.40 ± 3	96.02 ± 3	0.21	−25.50 ± 1
P-PBAT-Olig	170.40 ± 8	0.08	−26.00 ± 0.2	169.50 ± 7	0.06	−44.90 ± 1

Table 2 Non-photooxidized NP- and photooxidized P-PBAT-Olig assigned based on MALDI-TOF/TOF spectra. BA: butylene-adipate; BT: butylene-terephthalate; BH_2: butanediol; C_4H_{10}: butane; H_2O: water or hydroxyl and proton; CO: ketone group (C=O). The MALDI-TOF/TOF spectrum of PBAT-Olig chromatography peaks is available in the ESI† Fig. S1 for NP-PBAT-Olig and Fig. S2 for P-PBAT-Olig

NP-PBAT-Olig			P-PBAT-Olig		
Formula	Structure	Number of repeating units	Formula	Structure	Number of repeating units
$[(BA)_n]$	Cyclic	2/1–4	$[(BA)_n]$	Cyclic	2
$[(BA)_n\text{-}(C_4H_{10})]$	Linear	1–5/2	$[(BA)_n\text{-}(C_4H_{10})]$	Linear	2–4
$[(BA)_n\text{-}(BH_2)]$	Linear	1–8	$[(BA)_n\text{-}(BH_2)]$	Linear	2–9
$[(BA)_n\text{-}(BT)\text{-}(BH_2)]$	Linear	1–7/5–12	$[(BA)_n\text{-}(H_2O)]$	Linear	2–8
$[(BA)_n\text{-}(BT)]$	Cyclic	1–4/2–8	$[(BA)_n\text{-}(BH_2)\text{-}(CO)]$	Linear	2–7
$[(BA)_n\text{-}(BT)_2\text{-}(BH_2)]$	Linear	3–10	$[(BA)_n\text{-}(H_2O)\text{-}(CO)]$	Linear	2–6
$[(BA)_n\text{-}(BT)_3\text{-}(BH_2)]$	Linear	2–9/4–11	$[(BA)_n\text{-}(BT)\text{-}(BH_2)]$	Linear	1–8
$[(BA)_n\text{-}(BT)\text{-}(C_4H_{10})]$	Linear	2–6	$[(BA)_n]$	Cyclic	2–6
$[(BA)_n\text{-}(BT)_2]$	Cyclic	0–5/8–10/3–9	$[(BA)_n\text{-}(BT)]$	Cyclic	1–3
$[(BA)_n\text{-}(BT)_4\text{-}(BH_2)]$	Linear	2–7/7–13/6–12	$[(BA)_n\text{-}(C_4H_{10})]$	Linear	2–9
$[(BA)_n\text{-}(BT)_7\text{-}(BH_2)]$	Linear	3–8	$[(BA)_n\text{-}(BT)\text{-}(C_4H_{10})]$	Linear	2–4
$[(BA)_n\text{-}(BT)_6\text{-}(BH_2)]$	Linear	5–9	$[(BA)_n\text{-}(BT)\text{-}(BH_2)]$	Linear	2–10
$[(BA)_n\text{-}(BT)_2\text{-}(C_4H_{10})]$	Linear	3–7	$[(BA)_n\text{-}(BT)_2\text{-}(BH_2)]$	Linear	2–5
$[(BA)_n\text{-}(BT)_3]$	Cyclic	0–8/1–5	$[(BA)_n\text{-}(BT)\text{-}(H_2O)]$	Linear	2–7
$[(BA)_n\text{-}(BT)_5\text{-}(BH_2)]$	Linear	3–9	$[(BA)_n\text{-}(BT)_2]$	Cyclic	1–7
$[(BA)_n\text{-}(BT)_4\text{-}(BH_2)]$	Linear	6–12	$[(BA)_n\text{-}(BT)]$	Cyclic	2–8
$[(BA)_n\text{-}(BT)_3\text{-}(BH_2)]$	Linear	11–14	$[(BA)_n\text{-}(BT)_4\text{-}(H_2O)]$	Linear	1–4
$[(BA)_n\text{-}(BT)_9\text{-}(BH_2)]$	Linear	2–5	$[(BA)_n\text{-}(BT)\text{-}(C_4H_{10})]$	Linear	6–11
$[(BA)_n\text{-}(BT)_7\text{-}(BH_2)]$	Linear	8–11	$[(BA)_n\text{-}(BT)_3\text{-}(BH_2)\text{-}(CO)]$	Linear	8–13
$[(BA)_n\text{-}(BT)_2\text{-}(C_4H_{10})]$	Linear	6–9	$[(BA)_n\text{-}(BT)_5\text{-}(C_4H_{10})]$	Linear	2–6
$[(BA)_n\text{-}(BT)_3\text{-}(C_4H_{10})]$	Linear	4–8	$[(BA)_n\text{-}(BT)_3\text{-}(BH_2)]$	Linear	4–9
$[(BA)_n\text{-}(BT)\text{-}(C_4H_{10})]$	Linear	8–13	$[(BA)_n\text{-}(BT)_4\text{-}(BH_2)]$	Linear	5–9
$[(BA)_n\text{-}(BT)_5\text{-}(BH_2)]$	Linear	6–11	$[(BA)_n\text{-}(BT)_4\text{-}(BH_2)]$	Linear	6–12
$[(BA)_n\text{-}(BT)_6\text{-}(BH_2)]$	Linear	4–7	$[(BA)_n\text{-}(BT)_2\text{-}(BH_2)\text{-}(CO)]$	Linear	5–7
$[(BA)_n\text{-}(BT)_5]$	Cyclic	2–5/6–9	$[(BA)_n\text{-}(BT)_6\text{-}(BH_2)]$	Linear	5–8
$[(BA)_n\text{-}(BT)\text{-}(H_2O)]$	Linear	2–9	$[(BA)_n\text{-}(BT)_2\text{-}(H_2O)]$	Linear	6–11
$[(BA)_n\text{-}(BT)_2\text{-}(H_2O)]$	Linear	1–8	$[(BA)_n\text{-}(BT)_3]$	Cyclic	1–5
$[(BA)_n\text{-}(BT)_4]$	Cyclic	0–9	$[(BA)_n\text{-}(BT)_2]$	Cyclic	4–8
$[(BA)_n\text{-}(BT)_6]$	Cyclic	7–11	$[(BA)_n\text{-}(BT)_4\text{-}(BH_2)]$	Linear	6–7
$[(BA)_n\text{-}(BT)_7\text{-}(H_2O)]$	Linear	2–4	$[(BA)_n\text{-}(BT)_5\text{-}(BH_2)]$	Linear	5
$[(BA)_n\text{-}(BT)_7]$	Cyclic	6–9	$[(BA)_n\text{-}(BT)_3]$	Cyclic	0–7
$[(BA)_n\text{-}(BT)_8]$	Cyclic	5–6	$[(BA)_n\text{-}(BT)_3\text{-}(CH_3OH)]$	Linear	0–7
$[(BA)_n\text{-}(BT)_4\text{-}(H_2O)]$	Linear	2–9	$[(BA)_n\text{-}(BT)_2]$	Linear	8–10
$[(BA)_n\text{-}(BT)_3\text{-}(H_2O)]$	Linear	4–10	$[(BA)_n\text{-}(BT)_5\text{-}(BH_2)]$	Linear	5–8
$[(BA)_n\text{-}(BT)_6]$	Cyclic	0–8/6–8	$[(BA)_n\text{-}(BT)_4\text{-}(BH_2)]$	Linear	8–9

NP-PBAT-Olig (Fig. S2A†). In both cases, it was the most abundant and smallest oligomer observed. The proportion of carbonyl/hydroxyl groups appearing on the polymeric series increased after photooxidation from 11% in NP-PBAT-Olig up to 26% in P-PBAT-Olig. The butylene-terephthalate (BT) was found to be randomly distributed in the polymer. The BT occurrence frequency was approximately 20% more frequent in the NP-PBAT-Olig with respect to the P-PBAT-Olig one. As shown in Fig. S4,† the increase of BT units in the oligomers positively correlated ($R^2 \simeq 0.86$) with the time retained in the HPLC; therefore, it is correlated with the hydrophobicity. From the NP-PBAT-Olig, eight consecutive peaks were obtained after 20 min run, while only six peaks from the P-PBAT-Olig were obtained after the same time.

3.2 Effects of NP- and P-PBAT-NPLs and NP- and P-PBAT-Olig on physiological endpoints of *C. reinhardtii*

Exposure of *C. reinhardtii* to NP- and P-PBAT-NPLs and NP- and P-PBAT-Olig for 72 h did not significantly alter the growth (Fig. S5†) and chlorophyll content (Fig. S6†) of the microalga (Dunnett's test, $p < 0.05$); thus, the highest observed-no-effect concentration (HONEC) was 50 mg L^{-1} PBAT-NPLS and PBAT-Olig. Raw data are available in the ESI† (Table S3 and S4). Although no significant effects were found on the growth of the alga when exposed for 72 h to NP- and P-PBAT-NPLs and NP- and P-PBAT-Olig (short-term exposure), sublethal effects could be happening that in the long term may cause damage to the cells; to shed light on that, mechanisms of toxic action were investigated. One of the common responses reported in ecotoxicological studies involving NPLs is the formation of reactive oxygen species (ROS) and oxidative stress. ROS overproduction can lead to an imbalance between intracellular ROS species and the antioxidant mechanisms of the cell. To investigate whether NP- and P-PBAT-NPL and NP- and P-PBAT-Olig treatments could induce ROS formation and eventually oxidative stress in *C. reinhardtii* cells, flow cytometry (FCM) analyses to assess the formation of H_2O_2 using the fluorescent dye DHR123 were performed. Results showed a significant increase in H_2O_2 intracellular levels (129%; $p < 0.01$) after 72 h

exposure to 0.01 mg L^{-1} NP-PBAT-NPLs, the lowest tested concentration (Fig. 3A). This response appeared to increase constantly at concentrations ranging from 1 mg L^{-1} (122%; $p <$ 0.05), to 10 mg L^{-1} (135%; $p < 0.001$) and 50 mg L^{-1} (154%; $p <$ 0.001) (in Fig. 3B, cell subpopulations P1 in green are healthy cells and P2 in blue are cells affected by ROS overproduction).
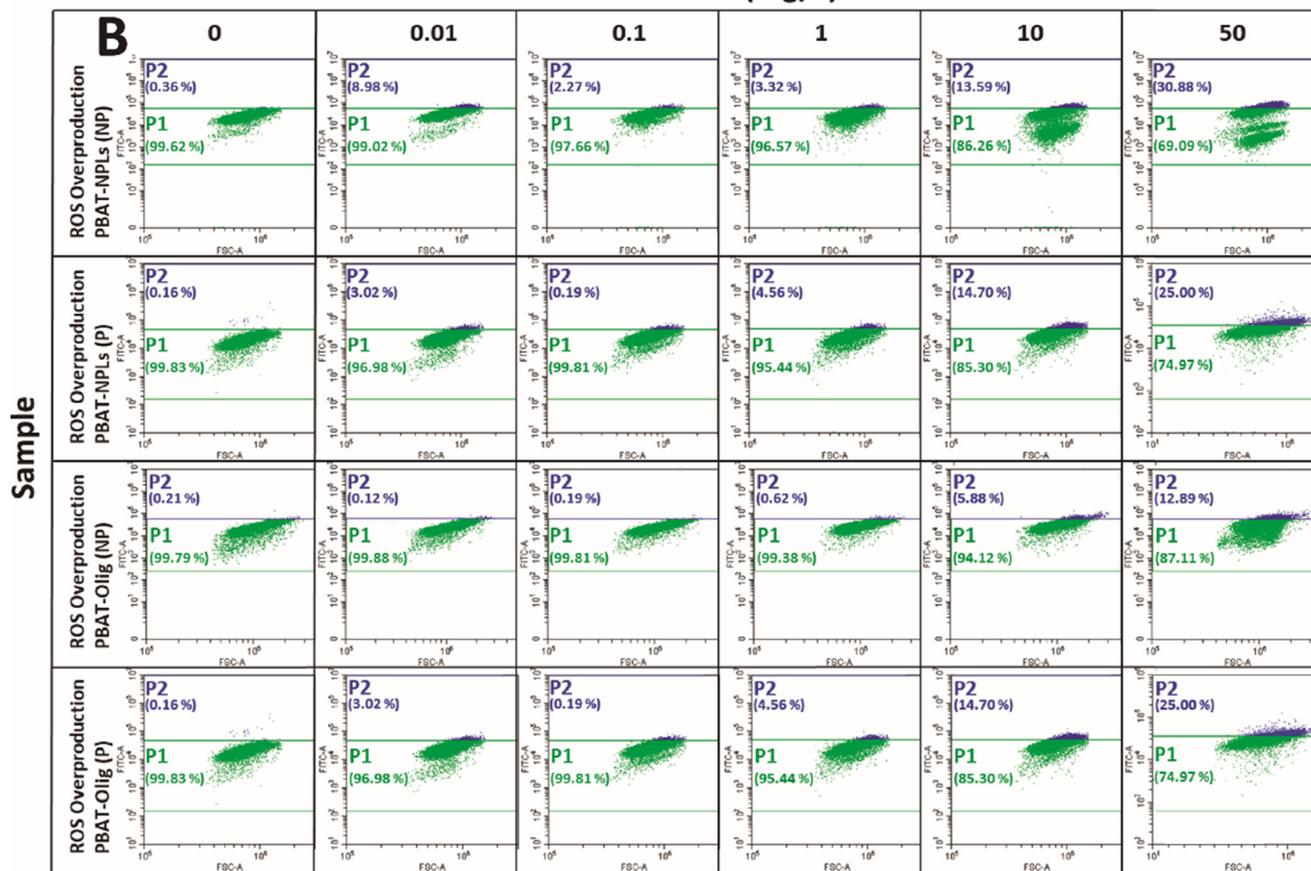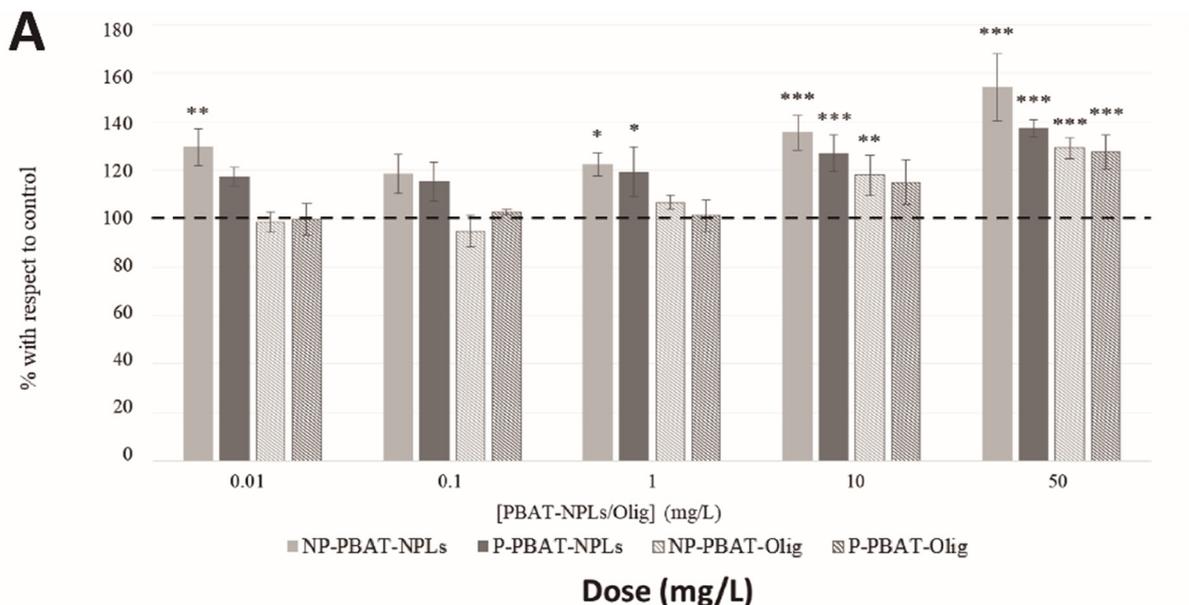
Fig. 3 A) Percentage of variation with respect to the control using the mean of fluorescence intensity for ROS production after exposure to NP- and P-PBAT-NPLs and NP- and P-PBAT-Olig. Asterisks indicate treatments that are significantly different (Dunnett's test, (***) $p < 0.001$; (**) $p <$ 0.01; (*) $p < 0.05$) from the control represented as 100% (dotted line). B) Representative flow cytometry dot-plots showing ROS overproduction in *C. reinhardtii* after 72 h exposure to NP- and P-PBAT-NPLs and NP- and P-PBAT-Olig; reactive oxygen species (ROS) were assessed in P1 in green (healthy cells) and P2 in blue (cells affected by ROS overproduction). Raw data are available in the ESI† (Table S5).
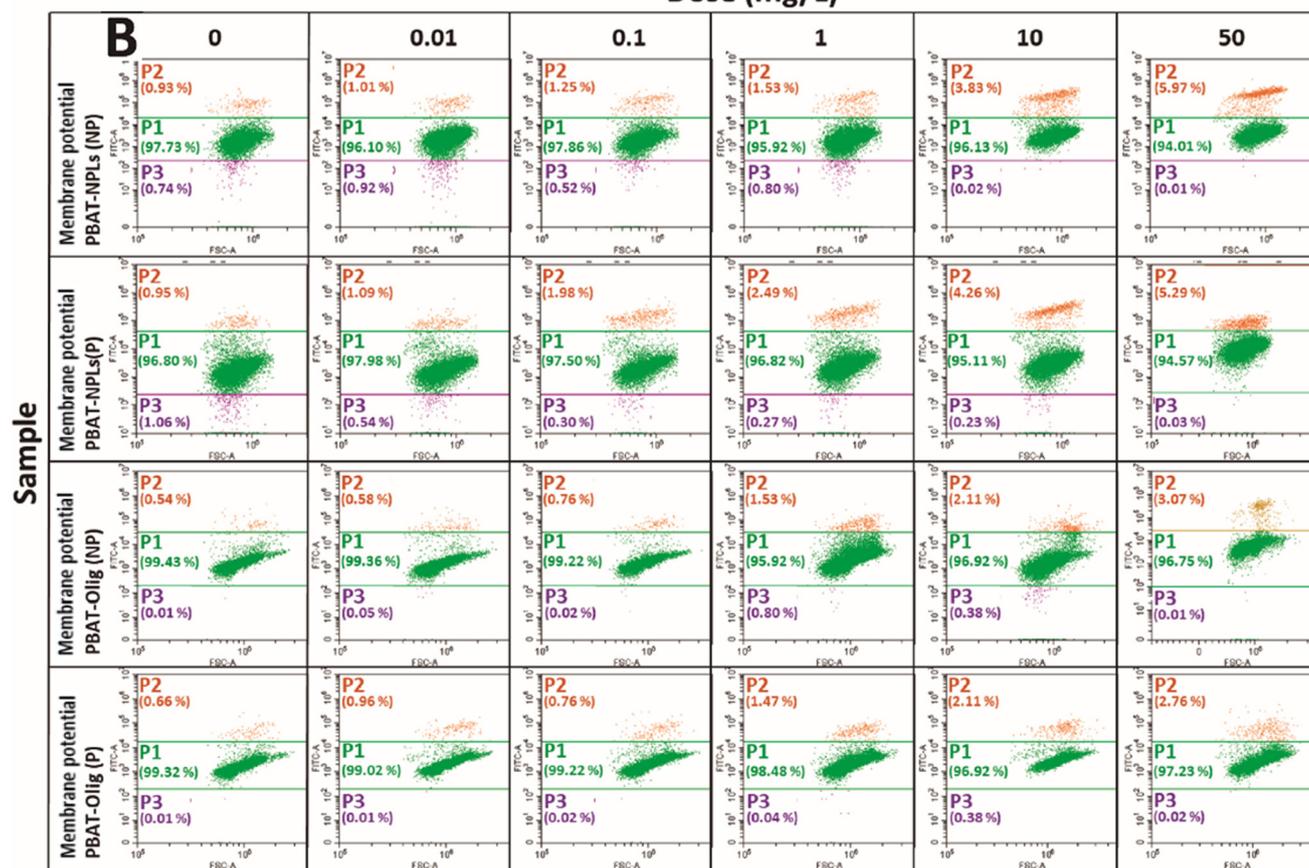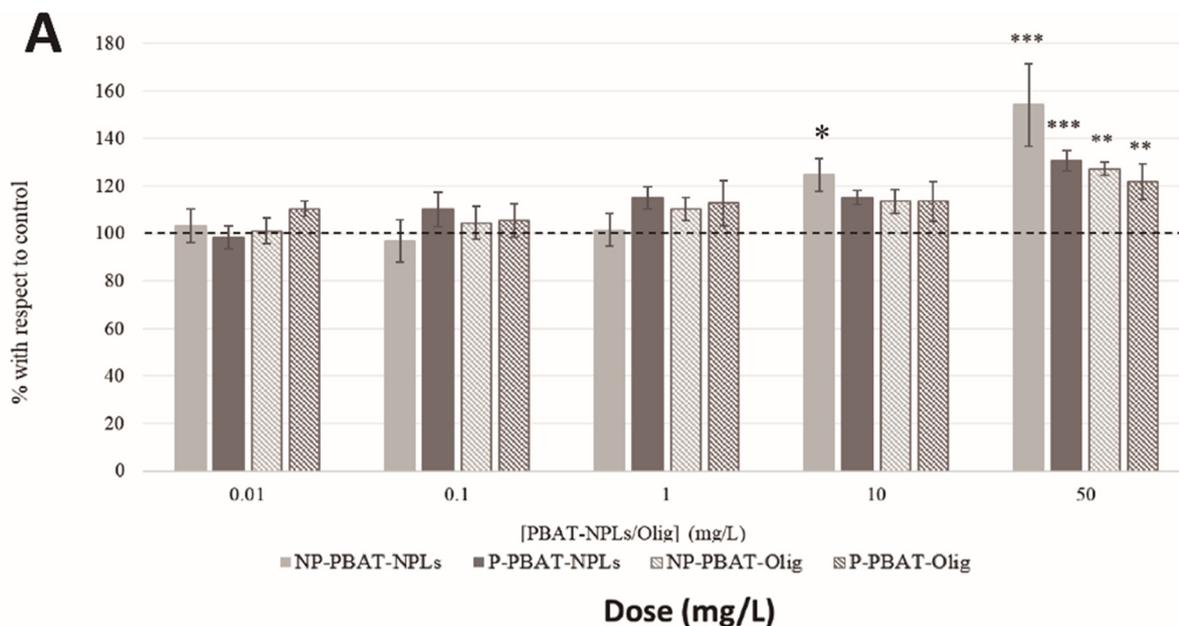
This journal is © The Royal Society of Chemistry 2025

Environ. Sci.: Nano, 2025, **12**, 1150–1165 | 1157

Fig. 4 A) Percentage of variation with respect to the control using the mean of fluorescence intensity for membrane depolarization after exposure to NP- and P-PBAT-NPLs and NP- and P-PBAT-Olig. Asterisks indicate treatments that are significantly different (Dunnett's test, (***) $p <$ 0.001; (**) $p < 0.01$; (*) $p < 0.05$) from the control represented as 100% (dotted line). B) Representative flow cytometry dot-plots showing alterations of the membrane potential in *C. reinhardtii* after 72 h exposure NP- and P-PBAT-NPLs and NP- and P-PBAT-Olig; cytoplasmatic membrane potential was assessed in three gates: P1 in green (healthy cells), P2 in orange (cells affected by membrane depolarization) and P3 in purple (cells affected by membrane hyperpolarization). Raw data are available in the ESI† (Table S6).

P-PBAT-NPLs caused similar alterations in H_2O_2 intracellular levels, causing a significant and constant increase at 1 mg L^{-1} (119%; $p < 0.05$), 10 mg L^{-1} (127%; $p < 0.001$), and 50 mg L^{-1} (137%; $p < 0.001$) (Fig. 3A). Nevertheless, ROS formation

(hydrogen peroxide) increased to a lesser extent when cells were exposed to NP- and P-PBAT-Olig. The oligomeric fraction only caused a significant ROS overproduction at 10 mg L^{-1} (118%; $p < 0.01$) with further increases at 50 mg L^{-1} (129%; $p < 0.001$) in the case of NP-PBAT-Olig, and at 50 mg L^{-1} (128%; $p < 0.001$) after P-PBAT-Olig exposure (Fig. 3A).

The cytoplasmatic membrane potential has also been analysed by FCM using the fluorochrome $DiBAC_4(3)$ (Fig. 4). A significant increase in $DiBAC_4(3)$-stained cells is indicative of a greater fluorochrome influx to the cells; this uptake of $DiBAC_4(3)$ indicates membrane depolarization. Our results showed an increase in membrane depolarization after cell exposure for 72 h in all treatments, with this increase being significant at 10 mg L^{-1} for NP-PBAT-NPLs (125%; $p < 0.05$) and at the highest tested concentration, 50 mg L^{-1} for NP- (154%; $p < 0.001$) and P- (131%; $p < 0.001$) PBAT-NPLs, and NP- (127%; $p < 0.01$) and P- (122%; $p < 0.01$) PBAT-Olig respectively (Fig. 4A) (in Fig. 4B, cell subpopulations P1 in green are healthy cells, P2 in orange are cells affected by membrane depolarization and P3 in purple are cells affected by membrane hyperpolarization). No significant decrease in fluorescence was observed, therefore, the exposure did not cause membrane hyperpolarization of the microalga.

ROS overproduction can trigger lipid peroxidation by attacking carbon–carbon double bonds in lipids. Due to their double bonds, polyunsaturated lipids, which are principal components of cell membranes, are prone to oxidant attack, leading to malondialdehyde (MDA) formation as a predominant by-product. The MDA content can be measured by its reaction with thiobarbituric acid (TBA), which leads to the formation of MDA-TBA2, so called TBARS, a conjugate that absorbs in the visible spectrum at 532 nm and produces a red-pink colour. Thus, an increase in TBARS (expressed here as the percentage of MDA) is associated with membrane lipid peroxidation.

As shown in Fig. 5, a significant increase in MDA levels was caused by the exposure of algal cells to all treatments, with a significant increase at 10 mg L^{-1} (141%; $p < 0.05$) and 50 mg L^{-1} (152%; $p < 0.05$) for NP-PBAT-NPLs and 50 mg L^{-1} (145%; $p < 0.05$) for P-PBAT-NPLs. Regarding exposure of cells to PBAT-Olig, both NP- and P induced a slight but non-significant increase in MDA levels for 50 mg L^{-1} exposure (128% and 127%; $p < 0.05$ for NP- and P-PBAT-Olig, respectively).
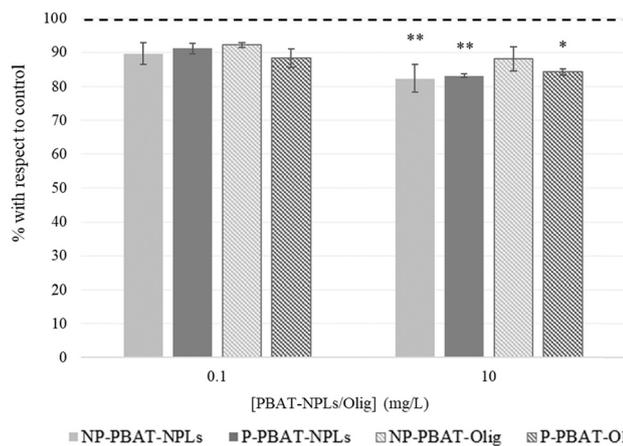
The main physiological function of *C. reinhardtii* cells is photosynthesis, therefore, to investigate whether NP- and P-PBAT-NPLs and NP- and P-PBAT-Olig had any effect on this crucial parameter, the photosynthetic activity measured as oxygen evolution in two sublethal intermediate concentrations of NP- and P-PBAT-NPLs and NP- and P-PBAT-Olig was evaluated. The two chosen concentrations were 0.1 mg L^{-1}, which already caused significant ROS overproduction but still without an effect on the membrane potential and lipid peroxidation levels, and 10 mg L^{-1}, which caused alterations in these parameters. These concentrations were used to test the effects of 72 h cell exposure to NP- and P-PBAT-NPLs and NP- and P-PBAT-Olig (Fig. 6). All the treatments caused a decrease ~10% ($p > 0.05$) in photosynthetic activity at 0.1 mg L^{-1} exposure by 72 h and a significant decrease of ~16% ($p < 0.01$ for NP- and P-PBAT-NPLs; $p < 0.05$ for P-PBAT-Olig) at 10 mg L^{-1}. This decrease was not observed after exposure to NP-PBAT-Olig.

Some authors have reported a relationship between pollutant exposure and the cell size increase in *C. reinhardtii* cells. We selected the two intermediate concentrations (0.1 and 10 mg L^{-1}) to test the effects of 72 h exposure to NP- and P-PBAT-NPLs and NP- and P-PBAT-Olig on *C. reinhardtii* cells. As can be seen in Fig. 7, *C. reinhardtii* cells treated with 0.1
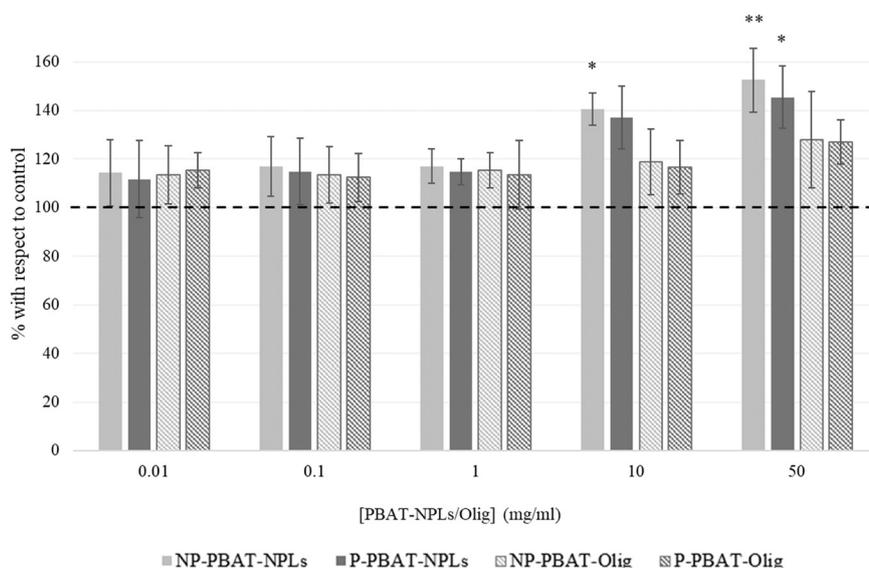
Fig. 5 Lipid peroxidation, measured by the thiobarbituric acid reactive substance method (TBARS), on *C. reinhardtii* after 72 h exposure to NP- and P-PBAT-NPLs and NP- and P-PBAT-Olig. Asterisks indicate treatments that are significantly different (Dunnett's test, (***) $p < 0.001$; (**) $p < 0.01$; (*) $p < 0.05$) from the control represented as 100% (dotted line). Raw data are available in the ESI† (Table S7).

This journal is © The Royal Society of Chemistry 2025

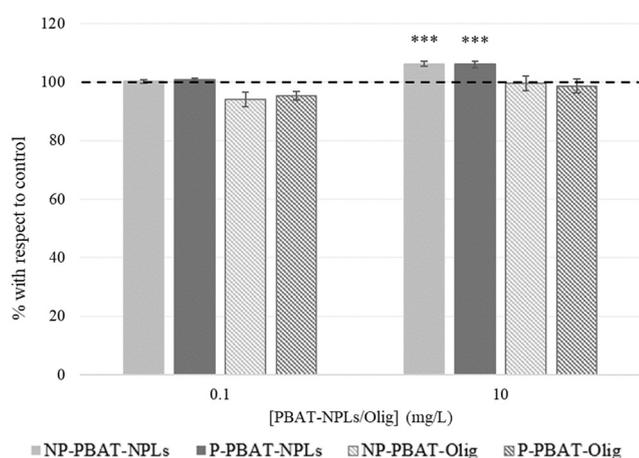*Environ. Sci.: Nano*, 2025, **12**, 1150–1165 | 1159

Fig. 6 Oxygen evolution of *C. reinhardtii* after 72 h exposure to NP- and P-PBAT-NPLs and NP- and P-PBAT-Olig. Asterisks indicate treatments that are significantly different (Dunnett's test, (***) $p < 0.001$; (**) $p < 0.01$; (*) $p < 0.05$) from the control represented as 100% (dotted line). Raw data are available in the ESI† (Table S8).

mg L^{-1} NP- (Fig. S7B†) and P- (Fig. S7E†) PBAT-NPLs showed no significant differences in cell size; however, there was a significant cell size increase after exposure to 10 mg L^{-1} NP- (Fig. S7C†) and P- (Fig. S7F†) PBAT-NPLs (106%; $p < 0.05$). No differences in cell size were observed for exposure to 0.1 and 10 mg L^{-1} of NP- and P-PBAT-Olig (Fig. 7).

Overall, short term (72 h) exposure of *C. reinhardtii* to NP-PBAT-NPLs provoked significant ROS overproduction at the lowest concentration tested of 0.01 mg L^{-1} (Fig. 3; Table S5†) and NP- and P-PBAT-NPLs caused significant membrane depolarization (Fig. 4; Table S6†), lipid peroxidation (Fig. 5; Table S7†), impaired photosynthesis (Fig. 6; Table S8†) and increase of the cell size (Fig. 7 and S7; Table S9†) at 10 mg L^{-1}. NP- and P-PBAT-Olig showed fewer toxic effects but

Fig. 7 Cell size based on flow cytometry back scattering of *C. reinhardtii* after 72 h exposure to NP- and P-PBAT-NPLs and NP- and P-PBAT-Olig. Asterisks indicate treatments that are significantly different (***) $p < 0.001$; (**) $p < 0.01$; (*) $p < 0.05$ from the control represented as 100% (dotted line). Raw data of cell size based in flow cytometry are available in the ESI† (Table S9).

triggered significant ROS overproduction (Fig. 3; Table S5†) and membrane depolarization (Fig. 4; Table S6†) at the highest concentration tested of 50 mg L^{-1}, and P-PBAT-Olig impaired photosynthesis (Fig. 6; Table S8†) at 10 mg L^{-1}. All these alterations in the long term may cause significant damage to the algal cells that may compromise their viability eventually causing a detrimental effect on the aquatic trophic chain.

4 Discussion

In this work, both non-photooxidized and photooxidized secondary NPLs were successfully produced using a highly efficient method, yielding 0.199 mg of secondary NP-PBAT-NPLs per gram of PBAT-microbeads These yields are comparable to those reported in previous studies ranging from 0.09 to 0.25 mg g^{-1} of NPLs below 100 nm.[30] The capability to produce sufficient quantities of NPLs, particularly those other than PS, is crucial for advancing toxicity testing and might be useful for developing standardized protocols for NPL detection in real samples. Moreover, this method enables the production of dry PBAT-NPLs and PBAT-Olig, allowing for storage and subsequent resuspension at the desired concentration in any testing culture media. This contrasts with other methods where NPLs are resuspended in water,[29,30] which subjects them to hydrolytic degradation during the process, complicating storage. Additionally, our method avoids the use of surfactants to maintain particle dispersion replacing them with ethanol as suggested by the programme NANoREG for a common European approach to the regulatory testing of nanomaterials.[54] This is significant as surfactants can influence ecotoxicological assessments.[55] Despite the absence of surfactants, stable NPL suspensions were achieved, as evidenced by a ζ-potential of less than −30 mV. The hydrodynamic size of PBAT-NPLs was < 70 nm, which is smaller than those reported in previous studies, for instance using cryomilling,[56] and highly relevant especially in the phytotoxicology field considering recent outcomes regarding the microalgal differential uptake for NPLs < 100 nm.[57] Thus, a key advantage of the method presented here is that it generates NPLs without the need for prior photooxidation, unlike other techniques that rely on photodegradation processes.

The oligomeric fraction was also efficiently produced and isolated with a yield of 10.275 mg of NP-PBAT-Olig per gram of PBAT-microbeads. Olig have been defined based on the degree of polymerization (<40 units) or the molecular weight (<10 kDa) and they have been detected during washing of polyester textiles.[58] However, these oligomers (with a mean size of 94–170 nm) fall within the size range classified as NPLs in this study, due to their hydrophobic-driven self-aggregation in aqueous media. These sizes might vary depending on the surrounding environment and therefore, they may behave as individual molecules in contact with biological membranes.[10] In our previous research, Olig were defined as molecules <50 kDa,[8] in which yields reaching up to 3.17 mg of PCL-Olig per gram of PCL-microbeads after 132

days under hydrolytic and non-UV photodegradation conditions in water were obtained. The method presented here is faster and enables the production of purified isolated oligomers without photodegradation. Analysis of the oligomeric fraction by FTIR indicates the presence of characteristic C=O stretching peaks. The difference between NPLs and the oligomers is the combination, in the case of the oligomers, of the 1732 cm^{-1} and 1720 cm^{-1} peaks (corresponding to the C=O stretching vibration in the amorphous and crystalline regions of the polymer, respectively) in one single peak. The combination of these peaks has been reported in other semicrystalline biodegradable polymers like poly-ε-caprolactone as a consequence of the loss of the solid state, where crystalline and amorphous regions are lacking.[59] Furthermore, for the ecotoxicology field, a novel characterization approach was employed, involving the separation of the oligomeric chains by polarity dependence on the hydrocarbon chain length and monomer composition, specifically the presence of butylene-terephthalate units (as shown in Fig. S2 and S3†). This was followed by individual MALDI-TOF/TOF analysis of each separated peak, preventing low-mass saturation of the detector.[60] The applied approach allowed us to precisely identify both linear and cyclic oligomers, including their formula, structures, and number of repeating units. Thus, this approach allowed the comparison between the oligomeric lengths, which were shorter for the P-PBAT oligomer compared to the non-photooxidized ones and indicated the potentially higher abundance of the smallest oligomers, such as cyclic dimers or trimers, as a result of the photooxidation exposure, with this fraction being the most abundant in both samples. This detailed characterization is significant as it provides exact information on the oligomeric composition, enabling the testing of specific oligomer fractions separately. While some studies have highlighted the effects of certain biodegradable and non-biodegradable plastic derived oligomers,[10,61,62] the structures and fundamental properties of oligomers generated from most polymers are still poorly understood. Despite their potential ubiquity,[63] to date, secondary oligomers generated from plastics have been overlooked or poorly investigated, without acquiring their critical compositional information,[64] which, however, has been partially obtained for those present in non-degraded plastics together with additives and other leachates.[42]

The present study provides novel evidence on the impact of secondary NPLs generated from biodegradable plastics such as PBAT on freshwater primary producers; although there are several studies of the effect of NPLs on these organisms, fundamentally cyanobacteria and green algae, they have been mostly done using primary NPLs, basically polystyrene ones with a specific size and shape (usually spherical), and for these reasons, their environmental relevance is unclear.[65–74] When using as toxicity endpoints general parameters such as growth and the chlorophyll content, there were no significant differences between the effects of photooxidized and non-photooxidized NPLs (p values were 0.170 and 0.278 for the lowest and the highest concentrations, respectively); however, a slight difference in ROS production values was observed for NP and P-PBAT-NPLs mainly at the lowest and highest concentrations tested of 0.01 and 50 mg L^{-1} respectively. These differences were not significant (p = 0.170 for 0.01 mg L^{-1} and p = 278 for 50 mg L^{-1}) between photooxidized and non-photooxidized NPL treatments which could be due to the slightly higher ζ-potential of the non-protoxidized NPLs that may preserve a more dispersed colloidal suspension, increasing bioavailability and consequently the observed trend to provoke higher toxicity. Furthermore, photooxidized NPLs tend to be more unstable when co-exposed together with organic matter and divalent ions[75] that were present in the culture medium (Ca^{2+} and Mg^{2+}); thus, addition of the presence of exopolysaccharides and other organic substances released by the cells could have provoked a decrease of the stability of P-PBAT-NPLs and therefore their bioavailability explaining the differences seen in ROS overproduction between photooxidized and non-photooxidized NPLs. Regarding mechanisms of toxic actions on the green alga, PBAT-NPLs, both photooxidized and non-photooxidized, induced ROS overproduction in the alga at the lowest concentrations tested (*e.g.*, 0.01 mg L^{-1} and 1 mg L^{-1}), which are environmentally relevant since concentrations up to 1588 μg L^{-1} have been quantified in a Swedish lake[17] meaning that these NPLs might pose a threat to primary producers in freshwater; besides, the estimated increase of fragmentation of larger plastic fractions in the environment might result in the number of NPs in natural ecosystems being possibly even much higher than that of microplastics.[47] An increase in the level of ROS is a common initial response to NPLs in primary producers such as algae and cyanobacteria.[7,8,67,68,72–74] The observed increase in ROS levels is consistent with the lipid peroxidation and concomitant membrane integrity damage and is also consistent with photosynthetic activity inhibition as reported in previous studies.[7,72,76,77] In the long term, even when algal cells are exposed to low NPL concentrations, sustained oxidative damage, particularly if cells are unable to restore the balance between ROS and antioxidant defences, as a result of NPL exposure may increase membrane disruption increasing non-specific ion permeability[7,8,68,69,72] and lead to continued damage of the photosynthetic machinery, consistent with the known effects of ROS on photosynthesis.[65,67–69,72,73] Despite the moderate knowledge concerning plastic oligomers considered as non-intentionally added substances (NIAS) in food contact materials, little is known about their impact on the environment.[45,64] The chemical formation of oligomers occurs during the polymerization process, either as a result of incomplete polymerization or due to thermal or hydrolytic degradation of polymer chains during the processing of the polymeric material or under conditions of use. The resulting oligomer profile can be highly complex, consisting of linear, branched, and cyclic species, each of which may exhibit different migration behaviour.[78] Due to the current awareness about the massive entrance of plastic waste into the

This journal is © The Royal Society of Chemistry 2025

Environ. Sci.: Nano, 2025, **12**, 1150–1165 | **1161**

environment, it is crucial to understand the processes driving its release as well as its ecotoxicity. The release under environmental soft conditions as well as the lower toxicity of the oligomeric fraction compared to the nanoparticulate fraction has been previously observed for secondary polycaprolactone (PCL) oligomers and NPLs assessed in two cyanobacteria. The higher toxicity exerted by the PCL-NPLs has been related to the physical abrasion that the particles may cause in comparison with the oligomers, a hypothesis supported by the greater cytoplasmic membrane depolarization caused by the PCL-NPLs in comparison with the PCL-Olig. Consistently, the results obtained in the present study show a higher toxicity of the nanoparticulate fraction, supported by cytoplasmic membrane depolarization and ROS overproduction, at lower concentrations with respect to the effect provoked by the oligomeric fraction. Interestingly, the observed decrease in photosynthetic activity, as measured by oxygen evolution, revealed a similar toxicity by both NPLs and oligomeric fractions, which could be due to the potential capability of the oligomers to cross the cytoplasmic membranes, due to their hydrophobic nature, endangering the photosynthetic function.[62] In this regard, a similar alteration caused by both fractions was observed in nitrogen fixation in a cyanobacterium exposed to secondary PCL NPLs and PCL oligomers.[8] The results presented in this study point towards a long-term impact of secondary NPLs and Olig on freshwater primary producers and possibly other components of the aquatic trophic chain, which merits further research. The study also emphasizes the need to develop protocols for generating sufficient quantities of reference NPLs of each polymer, including biodegradable polymers, as they may pose future environmental concerns. Additionally, it underscores the importance of investigating the generation of Olig and their impact on biota.

5 Conclusions

In the present work, an improved method for the production of secondary nanoplastics (NPLs) and oligomers by simulating different processes of abiotic degradation under controlled conditions has been proposed and may be useful for the generation of reference NPLs in sufficient quantities to study their impact on biota. The generation and characterization of generated oligomers might be also extremely useful to further characterize the complete fragmentation of larger plastic fractions in the environment and also assess their environmental impact. This method has been applied successfully for the generation of secondary photooxidized and non-photooxidized PBAT-NPLs and PBAT-Olig materials that have been utilized to test multiple ecotoxicological parameters in the green alga *C. reinhardtii* showing increased ROS overproduction that results in cytoplasmic membrane impairment and photosynthesis inhibition that may be detrimental in the long term even at realistic environmental concentrations which may further compromise the aquatic trophic chain. This study encourages the development of protocols to generate sufficient quantities

of reference NPLs of a variety of polymers including biodegradable polymers as they might not be entirely safe for the environment and the need to study the environmental impact of oligomers.

Data availability

The data supporting this article have been included as part of the ESI.†

Author contributions

Silvia Gómez-Kong: conceptualization and design; experimental work; writing. Miguel Tamayo-Belda: conceptualization and design; experimental work; writing. Gerardo Pulido-Reyes: conceptualization and design; writing. Miguel González-Pleiter: conceptualization and design; writing. Carlos Edo: conceptualization and design; writing and review of the final version of the manuscript. Irene Verdú: conceptualization and design; writing and review of the final version of the manuscript. Francisco Leganés: conceptualization and design; writing and review of the final version of the manuscript. Roberto Rosal: conceptualization and design; writing and review of the final version of the manuscript. Francisca Fernández-Piñas: conceptualization and design; writing and review of the final version of the manuscript.

Conflicts of interest

The authors declare no competing interest.

Acknowledgements

References

1 Plastics Europe E. S., Plastics – the fast Facts 2023 [Internet], *Plastics Europe*, 2023, [cited 2024 Jan 22], Available from: **https://plasticseurope.org/es/knowledge-hub/plastics-the-fast-facts-2023/**.

2 L. J. J. Meijer, T. Van Emmerik, R. Van Der Ent, C. Schmidt and L. Lebreton, More than 1000 rivers account for 80% of global riverine plastic emissions into the ocean, *Sci. Adv.*, 2021, **7**(18), eaaz5803.

3 L. C. M. Lebreton, J. Van Der Zwet, J. W. Damsteeg, B. Slat, A. Andrady and J. Reisser, River plastic emissions to the world's oceans, *Nat. Commun.*, 2017, **8**(1), 15611.

4 K. Zhang, A. H. Hamidian, A. Tubić, Y. Zhang, J. K. H. Fang and C. Wu, *et al.*, Understanding plastic degradation and microplastic formation in the environment: A review, *Environ. Pollut.*, 2021, **274**, 116554.

1162 | *Environ. Sci.: Nano*, 2025, **12**, 1150–1165

This journal is © The Royal Society of Chemistry 2025

5   Y. K. Song, S. H. Hong, S. Eo and W. J. Shim, The fragmentation of nano- and microplastic particles from thermoplastics accelerated by simulated-sunlight-mediated photooxidation, *Environ. Pollut.*, 2022, **311**, 119847.

6   H. P. Erickson, Size and Shape of Protein Molecules at the Nanometer Level Determined by Sedimentation, Gel Filtration, and Electron Microscopy, *Biol. Proced. Online*, 2009, **11**(1), 32–51.

7   M. González-Pleiter, M. Tamayo-Belda, G. Pulido-Reyes, G. Amariei, F. Leganés and R. Rosal, *et al.*, Secondary nanoplastics released from a biodegradable microplastic severely impact freshwater environments, *Environ. Sci.: Nano*, 2019, **6**(5), 1382–1392.

8   M. Tamayo-Belda, G. Pulido-Reyes, M. González-Pleiter, K. Martín-Betancor, F. Leganés and R. Rosal, *et al.*, Identification and toxicity towards aquatic primary producers of the smallest fractions released from hydrolytic degradation of polycaprolactone microplastics, *Chemosphere*, 2022, **303**(April), 134966.

9   A. Serrano-Lotina, R. Portela, P. Baeza, V. Alcolea-Rodriguez, M. Villarroel and P. Ávila, Zeta potential as a tool for functional materials development, *Catal. Today*, 2023, **423**, 113862.

10 M. Wang, Q. Li and C. Shi, Oligomer nanoparticle release from polylactic acid plastics catalysed by gut enzymes triggers acute inflammation, *Nat. Nanotechnol.*, 2023, **18**, 403–411.

11 L. M. Hernandez, N. Yousefi and N. Tufenkji, Are There Nanoplastics in Your Personal Care Products?, *Environ. Sci. Technol. Lett.*, 2017, **4**(7), 280–285.

12 H. Cai, E. G. Xu, F. Du, R. Li, J. Liu and H. Shi, Analysis of environmental nanoplastics: Progress and challenges, *Chem. Eng. J.*, 2021, **410**, 128208.

13 L. D. B. Mandemaker and F. Meirer, Spectro-Microscopic Techniques for Studying Nanoplastics in the Environment and in Organisms, *Angew. Chem.*, 2023, **135**, e202210494.

14 D. Kau, D. Materić, R. Holzinger, K. Baumann-Stanzer, G. Schauer and A. Kasper-Giebl, Fine micro- and nanoplastics concentrations in particulate matter samples from the high alpine site Sonnblick, Austria, *Chemosphere*, 2024, **352**, 141410.

15 D. Materić, H. A. Kjær, P. Vallelonga, J. L. Tison, T. Röckmann and R. Holzinger, Nanoplastics measurements in Northern and Southern polar ice, *Environ. Res.*, 2022, **208**, 112741.

16 D. Materić, R. Holzinger and H. Niemann, Nanoplastics and ultrafine microplastic in the Dutch Wadden Sea – The hidden plastics debris?, *Sci. Total Environ.*, 2022, **846**, 157371.

17 D. Materić, M. Peacock, J. Dean, M. Futter, T. Maximov and F. Moldan, *et al.*, Presence of nanoplastics in rural and remote surface waters, *Environ. Res. Lett.*, 2022, **17**(5), 054036.

18 D. Materić, E. Ludewig, D. Brunner, T. Röckmann and R. Holzinger, Nanoplastics transport to the remote, high-altitude Alps, *Environ. Pollut.*, 2021, **288**, 117697.

19 D. Materić, A. Kasper-Giebl, D. Kau, M. Anten, M. Greilinger and E. Ludewig, *et al.*, Micro- and Nanoplastics in Alpine Snow: A New Method for Chemical Identification and (Semi) Quantification in the Nanogram Range, *Environ. Sci. Technol.*, 2020, **54**(4), 2353–2359.

20 Q. Li, Y. Lai, P. Li, X. Liu, Z. Yao and J. Liu, *et al.*, Evaluating the Occurrence of Polystyrene Nanoparticles in Environmental Waters by Agglomeration with Alkylated Ferroferric Oxide Followed by Micropore Membrane Filtration Collection and Py-GC/MS Analysis, *Environ. Sci. Technol.*, 2022, **56**(12), 8255–8265.

21 Y. Xu, Q. Ou, M. Jiao, G. Liu and J. P. Van Der Hoek, Identification and Quantification of Nanoplastics in Surface Water and Groundwater by Pyrolysis Gas Chromatography–Mass Spectrometry, *Environ. Sci. Technol.*, 2022, **56**(8), 4988–4997.

22 Y. Xu, Q. Ou, X. Wang, F. Hou, P. Li and J. P. Van Der Hoek, *et al.*, Assessing the Mass Concentration of Microplastics and Nanoplastics in Wastewater Treatment Plants by Pyrolysis Gas Chromatography–Mass Spectrometry, *Environ. Sci. Technol.*, 2023, **57**(8), 3114–3123.

23 A. Chamas, H. Moon, J. Zheng, Y. Qiu, T. Tabassum and J. H. Jang, *et al.*, Degradation Rates of Plastics in the Environment, *ACS Sustainable Chem. Eng.*, 2020, **8**(9), 3494–3511.

24 C. Venâncio, I. Melnic, M. Tamayo-Belda, M. Oliveira, M. A. Martins and I. Lopes, Polymethylmethacrylate nanoplastics can cause developmental malformations in early life stages of Xenopus laevis, *Sci. Total Environ.*, 2022, **806**, 150491.

25 A. Santos, M. Oliveira, I. Lopes, M. Almeida and C. Venâncio, Polyhydroxybutyrate (PHB) nanoparticles modulate metals toxicity in Hydra viridissima, *Sci. Total Environ.*, 2024, **932**, 172868.

26 D. S. Vicentini, D. J. Nogueira, S. P. Melegari, M. Arl, J. S. Köerich and L. Cruz, *et al.*, Toxicological Evaluation and Quantification of Ingested Metal-Core Nanoplastic by Daphnia magna Through Fluorescence and Inductively Coupled Plasma-Mass Spectrometric Methods, *Environ. Toxicol. Chem.*, 2019, **38**(10), 2101–2110.

27 D. M. Mitrano, A. Beltzung, S. Frehland, M. Schmiedgruber, A. Cingolani and F. Schmidt, Synthesis of metal-doped nanoplastics and their utility to investigate fate and behaviour in complex environmental systems, *Nat. Nanotechnol.*, 2019, **14**(4), 362–368.

28 J. R. Peller, S. P. Mezyk, S. Shidler, J. Castleman, S. Kaiser and R. F. Faulkner, *et al.*, Facile nanoplastics formation from macro and microplastics in aqueous media, *Environ. Pollut.*, 2022, **313**, 120171.

29 P. Merdy, F. Delpy, A. Bonneau, S. Villain, L. Iordachescu and J. Vollertsen, *et al.*, Nanoplastic production procedure for scientific purposes: PP, PVC, PE-LD, PE-HD, and PS, *Heliyon*, 2023, **9**(8), e18387.

30 Y. Ji, C. Wang, Y. Wang, L. Fu, M. Man and L. Chen, Realistic polyethylene terephthalate nanoplastics and the size- and surface coating-dependent toxicological impacts on zebrafish embryos, *Environ. Sci.: Nano*, 2020, **7**(8), 2313–2324.

This journal is © The Royal Society of Chemistry 2025

Environ. Sci.: Nano, 2025, **12**, 1150–1165 | **1163**

31 M. T. Ekvall, M. Lundqvist, E. Kelpsiene, E. Šileikis, S. B. Gunnarsson and T. Cedervall, Nanoplastics formed during the mechanical breakdown of daily-use polystyrene products, *Nanoscale Adv.*, 2019, **1**(3), 1055–1061.

32 M. Tamayo-Belda, C. Venâncio, F. Fernandez-Piñas, R. Rosal, I. Lopes and M. Oliveira, Effects of petroleum-based and biopolymer-based nanoplastics on aquatic organisms: A case study with mechanically degraded pristine polymers, *Sci. Total Environ.*, 2023, **883**, 163447.

33 D. Magrì, P. Sánchez-Moreno, G. Caputo, F. Gatto, M. Veronesi and G. Bardi, *et al.*, Laser Ablation as a Versatile Tool To Mimic Polyethylene Terephthalate Nanoplastic Pollutants: Characterization and Toxicology Assessment, *ACS Nano*, 2018, **12**(8), 7690–7700.

34 Y. Ji, L. Chen, Y. Wang, J. Zhang, Y. Yu and M. Wang, *et al.*, Realistic Nanoplastics Induced Pulmonary Damage via the Crosstalk of Ferritinophagy and Mitochondrial Dysfunction, *ACS Nano*, 2024, **18**(26), 16790–16807.

35 M. Tamayo-Belda, G. Pulido-Reyes, R. Rosal and F. Fernández-Piñas, Nanoplastic toxicity towards freshwater organisms, *Water Emerging Contam. Nanoplast.*, 2022, **1**(4), 19.

36 G. McConnel, Z. A. Kasuske, C. Mazariegos-Ortíz, S. R. Muñoz and J. E. Cañas-Carrell, A systems perspective of terrestrial, aquatic, and human health impacts of non-polystyrene-based nanoplastics, *Curr. Opin. Environ. Sci. Health*, 2024, **39**, 100557.

37 A. Khan and Z. Jia, Recent insights into uptake, toxicity, and molecular targets of microplastics and nanoplastics relevant to human health impacts, *iScience*, 2023, **26**(2), 106061.

38 S. Kauts, S. Shabir, S. Yousuf, Y. Mishra, R. Bhardwaj and A. A. Milibari, *et al.*, The evidence of in-vivo and in-vitro studies on microplastic and nano plastic toxicity in mammals: A possible threat for an upcoming generation?, *Phys. Chem. Earth*, 2023, **132**, 103511.

39 D. Subramanian, G. Ponnusamy Manogaran and D. Dharmadurai, A systematic review on the impact of micro-nanoplastics on human health: Potential modulation of epigenetic mechanisms and identification of biomarkers, *Chemosphere*, 2024, **363**, 142986.

40 C. L. Bai, D. Wang, Y. L. Luan, S. N. Huang, L. Y. Liu and Y. Guo, A review on micro- and nanoplastics in humans: Implication for their translocation of barriers and potential health effects, *Chemosphere*, 2024, **361**, 142424.

41 C. Casella and S. J. Ballaz, Genotoxic and neurotoxic potential of intracellular nanoplastics: A review, *J. Appl. Toxicol.*, 2024, jat.4598.

42 L. Zimmermann, A. Dombrowski, C. Völker and M. Wagner, Are bioplastics and plant-based materials safer than conventional plastics? In vitro toxicity and chemical composition, *Environ. Int.*, 2020, **145**, 106066.

43 L. G. Pinaeva and A. S. Noskov, Biodegradable biopolymers: Real impact to environment pollution, *Sci. Total Environ.*, 2024, **947**, 174445.

44 M. Qin, C. Chen, B. Song, M. Shen, W. Cao and H. Yang, *et al.*, A review of biodegradable plastics to biodegradable microplastics: Another ecological threat to soil environments?, *J. Cleaner Prod.*, 2021, **312**, 127816.

45 M. Hoppe, P. De Voogt and R. Franz, Identification and quantification of oligomers as potential migrants in plastics food contact materials with a focus in polycondensates – A review, *Trends Food Sci. Technol.*, 2016, **50**, 118–130.

46 C. Zarna, S. Rodríguez-Fabià, A. T. Echtermeyer and G. Chinga-Carrasco, Preparation and characterisation of biocomposites containing thermomechanical pulp fibres, poly(lactic acid) and poly(butylene-adipate-terephthalate) or poly(hydroxyalkanoates) for 3D and 4D printing, *Addit. Manuf.*, 2022, **59**, 103166.

47 C. Sorasan, C. Edo, M. González-Pleiter, F. Fernández-Piñas, F. Leganés and A. Rodríguez, *et al.*, Generation of nanoplastics during the photoageing of low-density polyethylene, *Environ. Pollut.*, 2021, **289**, 117919.

48 J. Hurtado-Gallego, G. Pulido-Reyes, M. González-Pleiter, G. Salas, F. Leganés and R. Rosal, *et al.*, Toxicity of superparamagnetic iron oxide nanoparticles to the microalga Chlamydomonas reinhardtii, *Chemosphere*, 2020, **238**, 124562.

49 S. W. Jeffrey and G. F. Humphrey, New spectrophotometric equations for determining chlorophylls a, b, c1 and c2 in higher plants, algae and natural phytoplankton, *Biochem. Physiol. Pflanz.*, 1975, **167**(2), 191–194.

50 M. Tamayo-Belda, M. González-Pleiter, G. Pulido-Reyes, K. Martin-Betancor, F. Leganés and R. Rosal, *et al.*, Mechanism of the toxic action of cationic G5 and G7 PAMAM dendrimers in the cyanobacterium: Anabaena sp. PCC7120, *Environ. Sci.: Nano*, 2019, **6**(3), 863–878.

51 C. Ortega-Villasante, R. Rellán-Álvarez, F. F. Del Campo, R. O. Carpena-Ruiz and L. E. Hernández, Cellular damage induced by cadmium and mercury in Medicago sativa, *J. Exp. Bot.*, 2005, **56**(418), 2239–2251.

52 F. Leganés, F. Martínez-Granero, M. Á. Muñoz-Martín, E. Marco, A. Jorge and L. Carvajal, *et al.*, Characterization and responses to environmental cues of a photosynthetic antenna-deficient mutant of the filamentous cyanobacterium Anabaena sp. PCC 7120, *J. Plant Physiol.*, 2014, **171**(11), 915–926.

53 A. R. de Matos Costa, A. Crocitti, L. Hecker de Carvalho, S. C. Carroccio, P. Cerruti and G. Santagata, Properties of Biodegradable Films Based on Poly(butylene Succinate) (PBS) and Poly(butylene Adipate-co-Terephthalate) (PBAT) Blends, *Polymer*, 2020, **12**(10), 2317.

54 P. Jantunen, S. Gottardo and H. Crutzen, NANoREG Toolbox for the Safety Assessment of Nanomaterials [Internet], *European Commission, Joint Research Centre (JRC)*, 2017, [cited 2024 Jan 22], Available from: http://data.europa.eu/89h/jrc-nano-ehs-ring-nanoreg-tb.

55 O. Pikuda, E. G. Xu, D. Berk and N. Tufenkji, Toxicity Assessments of Micro- and Nanoplastics Can Be Confounded by Preservatives in Commercial Formulations, *Environ. Sci. Technol. Lett.*, 2019, **6**(1), 21–25.

56 C. J. McColley, J. A. Nason, B. J. Harper and S. L. Harper, An assessment of methods used for the generation and

characterization of cryomilled polystyrene micro- and nanoplastic particles, *Microplast. Nanoplast.*, 2023, **3**(1), 20.

57 Y. Wang, N. Yan, Q. Ji, S. Chen, Y. Huang, T. Y. Wong and J. Shi, Novel insights into the joint phytotoxicity of nanoplastics and silver ions at environmentally relevant concentrations: a dual aggregation-induced emission bioimaging approach, *Environ. Sci.:Nano*, 2024, **11**(11), 4521–4535.

58 T. Yang, Y. Xu, G. Liu and B. Nowack, Oligomers are a major fraction of the submicrometre particles released during washing of polyester textiles, *Nat. Water*, 2024, **2**(2), 151–160.

59 K. Phillipson, J. N. Hay and M. J. Jenkins, Thermal analysis FTIR spectroscopy of poly(ε-caprolactone), *Thermochim. Acta*, 2014, **595**, 74–82.

60 A. Westman, G. Brinkmalm and D. F. Barofsky, MALDI induced saturation effects in chevron microchannel plate detectors, *Int. J. Mass Spectrom. Ion Processes*, 1997, **169–170**, 79–87.

61 N. Yoshinaga, A. Tateishi, Y. Kobayashi, T. Kubo, H. Miyakawa and K. Satoh, *et al.*, Effect of Oligomers Derived from Biodegradable Polyesters on Eco- and Neurotoxicity, *Biomacromolecules*, 2023, **24**(6), 2721–2729.

62 J. Järvenpää, M. Perkkiö, R. Laitinen and M. Lahtela-Kakkonen, PE and PET oligomers' interplay with membrane bilayers, *Sci. Rep.*, 2022, **12**(1), 2234.

63 B. G. Kwon, K. Koizumi, S. Y. Chung, Y. Kodera, J. O. Kim and K. Saido, Global styrene oligomers monitoring as new chemical contamination from polystyrene plastic marine pollution, *J. Hazard. Mater.*, 2015, **300**, 359–367.

64 C. Shi, M. Wang, Z. Wang, G. Qu, W. Jiang and X. Pan, *et al.*, Oligomers from the Synthetic Polymers: Another Potential Iceberg of New Pollutants, *Environ. Health*, 2023, **1**(4), 228–235.

65 X. Li, H. Qiu, P. Zhang, L. Song, A. Romero-Freire and E. He, Role of heteroaggregation and internalization in the toxicity of differently sized and charged plastic nanoparticles to freshwater microalgae, *Environ. Pollut.*, 2023, **316**, 120517.

66 M. Déniel, F. Lagarde, A. Caruso and N. Errien, Infrared spectroscopy as a tool to monitor interactions between nanoplastics and microalgae, *Anal. Bioanal. Chem.*, 2020, **412**(18), 4413–4422.

67 W. Yang, P. Gao, Y. Nie, J. Huang, Y. Wu and L. Wan, *et al.*, Comparison of the effects of continuous and accumulative exposure to nanoplastics on microalga Chlorella pyrenoidosa during chronic toxicity, *Sci. Total Environ.*, 2021, **788**, 147934.

68 W. Yang, P. Gao, G. Ma, J. Huang, Y. Wu and L. Wan, *et al.*, Transcriptome analysis of the toxic mechanism of nanoplastics on growth, photosynthesis and oxidative stress of microalga Chlorella pyrenoidosa during chronic exposure, *Environ. Pollut.*, 2021, **284**, 117413.

69 S. Wang, M. Liu, J. Wang, J. Huang and J. Wang, Polystyrene nanoplastics cause growth inhibition, morphological damage and physiological disturbance in the marine microalga Platymonas helgolandica, *Mar. Pollut. Bull.*, 2020, **158**, 111403.

70 A. Reynolds, D. M. Giltrap and P. G. Chambers, Acute growth inhibition & toxicity analysis of nano-polystyrene spheres on Raphidocelis subcapitata, *Ecotoxicol. Environ. Saf.*, 2021, **207**, 111153.

71 Y. Yang, Y. Guo, A. M. O'Brien, T. F. Lins, C. M. Rochman and D. Sinton, Biological Responses to Climate Change and Nanoplastics Are Altered in Concert: Full-Factor Screening Reveals Effects of Multiple Stressors on Primary Producers, *Environ. Sci. Technol.*, 2020, **54**(4), 2401–2410.

72 M. Tamayo-Belda, J. José Vargas-Guerrero, K. Martín-Betancor, G. Pulido-Reyes, M. González-Pleiter and F. Leganés, *et al.*, Understanding nanoplastic toxicity and their interaction with engineered cationic nanopolymers in microalgae by physiological and proteomic approaches, *Environ. Sci.: Nano*, 2021, **8**(8), 2277–2296.

73 X. Zheng, Y. Yuan, Y. Li, X. Liu, X. Wang and Z. Fan, Polystyrene nanoplastics affect growth and microcystin production of Microcystis aeruginosa, *Environ. Sci. Pollut. Res.*, 2021, **28**(11), 13394–13403.

74 X. Xin, B. Chen, B. Péquin, P. Song, M. Yang and X. Song, *et al.*, Binary toxicity of polystyrene nanoplastics and polybrominated diphenyl ethers to Arctic Cyanobacteria under ambient and future climates, *Water Res.*, 2022, **226**, 119188.

75 F. Lian, Y. Han, Y. Zhang, J. Li, B. Sun and Z. Geng, *et al.*, Exposure Order to Photoaging and Humic Acids Significantly Modifies the Aggregation and Transformation of Nanoplastics in Aqueous Solutions, *Environ. Sci. Technol.*, 2023, **57**(16), 6520–6529.

76 A. Latifi, M. Ruiz and C. C. Zhang, Oxidative stress in cyanobacteria, *FEMS Microbiol. Rev.*, 2009, **33**(2), 258–278.

77 I. Verdú, M. González-Pleiter, F. Leganés, F. Fernández-Piñas and R. Rosal, Leaching of herbicides mixtures from pre-exposed agricultural plastics severely impact microalgae, *Chemosphere*, 2023, **326**, 138475.

78 A. Schaefer, V. A. Ohm and T. J. Simat, Migration from can coatings: Part 2. Identification and quantification of migrating cyclic oligoesters below 1000 Da, *Food Addit. Contam.*, 2004, **21**(4), 377–389.

This journal is © The Royal Society of Chemistry 2025

Environ. Sci.: Nano, 2025, **12**, 1150–1165 | 1165